ACS Catalysis

Research Article

pubs.acs.org/acscatalysis

Bismuth Oxybromide with Reasonable Photocatalytic Reduction Activity under Visible Light

Jun Shang,[†] Weichang Hao,*[,†,⊥] Xiaojun Lv,[‡] Tianmin Wang,[†] Xiaolin Wang,[⊥] Yi Du,[⊥] Shixue Dou,[⊥] Tengfeng Xie,[§] Dejun Wang,[§] and Jiaou Wang[∥]

[†]Center of Materials Physics and Chemistry, and Department of Physics, Beihang University, Beijing 100191, P. R. China

[‡]Key Laboratory of Photochemical Conversion and Optoelectronic Materials, and HKU-CAS Joint Laboratory on New Materials, Technical Institute of Physics and Chemistry, Chinese Academy of Sciences (CAS), Beijing 100190, P. R. China

[⊥]Institute for Superconducting and Electronic Materials, University of Wollongong, Wollongong NSW 2522, Australia

[§]College of Chemistry, Jilin University, Changchun 130012, P. R. China

[∥]Beijing Synchrotron Radiation Facility, Institute of High Energy Physics, Chinese Academy of Sciences, Beijing 100049, P. R. China

Supporting Information

ABSTRACT: The original bismuth-based oxyhalide, known as the Sillén family, is an important photocatalyst due to its high photocatalytic oxidation activity. Here, we report a bismuth-based photocatalyst, $Bi_{24}O_{31}Br_{10}$, with reasonable reduction activity. The photoreduction capability of $Bi_{24}O_{31}Br_{10}$ in H_2 evolution from water reduction is 133.9 μmol after 40 h under visible light irradiation. $Bi_{24}O_{31}Br_{10}$ presents the highest activity among Bi_2O_3, BiOBr, and $Bi_{24}O_{31}Br_{10}$ in photocatalytic reduction of the Cr (VI) test, and Cr (VI) ions are totally removed in 40 min. The Mott–Schottky test shows the bottom of the conduction band fits the electric potential requirements for splitting water to H_2. First-principles calculations indicate the conduction band of $Bi_{24}O_{31}Br_{10}$ mainly consists of hybridized Bi 6p and Br 4s orbitals, which may contribute to the uplifting of the conduction band.

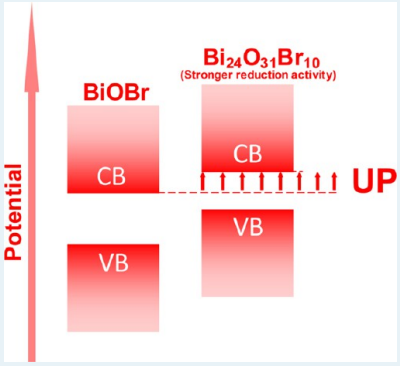

KEYWORDS: *bismuth-based oxyhalide, photocatalyst, $Bi_{24}O_{31}Br_{10}$, hydrogen production, photocatalytic reduction activity*

INTRODUCTION

Currently, the study of semiconductor photocatalysis is an important issue due to its potential applications in environmental pollution purification[1−5] and energy conversion.[6−10] Developing novel visible light photocatalysts with high activity is the primary task in this field. The bismuth-based compound, due to its special electronic structure, is a significant class of photocatalyst. For bismuth-based photocatalysts, Bi 6s and O 2p levels can form a preferable hybridized valence band (VB), which meets the potential requirement of organic oxidation.[11] Meanwhile, the hybridization of the Bi 6s and O 2p levels makes the VB largely dispersed, which favors the mobility of photoinduced holes in the VB[12] and is beneficial to the oxidation reaction. The original bismuth-based oxyhalide belongs to the Sillén family[13] expressed by bismuth oxide-based fluorite-like layers, $[M_2O_2]$, intergrown with single, double, or triple halide layers, $[X_1]$, $[X_2]$, or $[M_xX_3]$, producing compounds such as $LiBi_3O_4Cl_2$ (X_1), BiOCl (X_2), and $LiCa_2Bi_3O_4Cl_6$ (X_3). These Sillén compounds have been widely used as selective oxidation catalysts,[14] photocatalysts,[11] ferroelectric materials,[15] and pigments.[16] It is believed that the strong internal static electric fields perpendicular to the $[X_m]$ layer and the bismuth oxide-based fluorite-like layer enable the effective separation of the photoinduced electron–hole pairs. Many bismuth-based compounds with related Sillén structure, such as BiOX (X = Cl, Br, I),[17−19] $BiVO_4$,[11] $NaBiO_3$,[20] bismuth titanate,[21,22] and so forth, have been reported to perform with high photocatalytic oxidation activity. However, to the best of our knowledge, the photocatalytic reduction property of bismuth-based compounds, especially water reduction to evolve H_2, is rarely researched. Through a heavy doping strategy, BiOBr could be changed to $Bi_{24}O_{31}Br_{10}$ with the variation of hybridization and crystal structure. Recently, $Bi_{24}O_{31}Br_{10}$ has been reported to have considerable photocatalytic oxidation activity.[23,24] Here, its reduction activity attracts us.

$Bi_{24}O_{31}Br_{10}$ has its conduction band (CB) and VB formed from p or sp hybridization states, because Bi, O, and Br are all p-block elements. Photocatalysts that are only composed of p-block elements possess unique advantages. The anisotropic properties of the p state can lead to highly dispersive band structures in comparison with d states via sp hybridization.[25] The dispersive band structure means that the effective mass of an electron or hole is light (see Supplementary Figure S1), which is advantageous for the photoinduced charge carrier

Received: November 4, 2013
Revised: January 9, 2014
Published: February 10, 2014

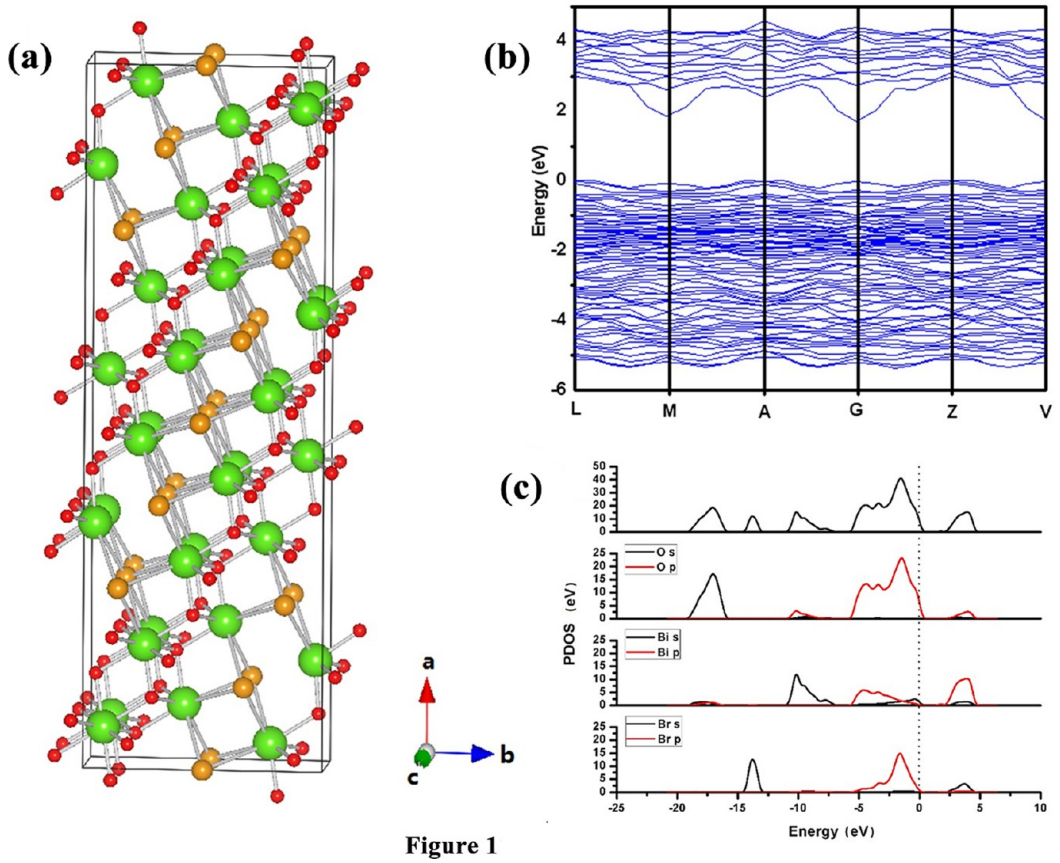

Figure 1

Figure 1. (a) Schematic diagram of crystal structure of $Bi_{24}O_{31}Br_{10}$: yellow, green, and red balls represent Bi, Br, and O, respectively. (b) Band structure of $Bi_{24}O_{31}Br_{10}$. (c) Calculated density of states (DOS) of $Bi_{24}O_{31}Br_{10}$.

transfer.[26−28] In the paper, the CB of $Bi_{24}O_{31}Br_{10}$ is found to be negative enough to split water to H_2. First-principles calculations show that the CB mainly consists of hybridized Bi 6p and Br 4s orbitals, which may contributes to the CB uplifting.

RESULTS AND DISCUSSION

$Bi_{24}O_{31}Br_{10}$ has a monoclinic crystal structure with space group $A12/m1$ (JCPDS 75-0888).[29] The crystal consists of neighboring BiO_5 polyhedra connected by the shared Br^- ions at the corners, as shown in Figure 1(a). The Bi, Br, and O atoms fit into a layered stacking model. The calculated band structure and density of states (DOS) are shown in Figure 1(b), (c). The CB of $Bi_{24}O_{31}Br_{10}$ mainly consists of hybridized Bi 6p and Br 4s orbitals, whereas the VB mainly comes from hybridized Br 4p and O 2p orbitals. The bottom of the CB and the top of the VB are only constructed from sp and p states, leading to a charge transfer between p and sp states as expected. Furthermore, the hybridization of sp orbitals leads to a dispersive CB, which is beneficial for the transport of photoexcited charge carriers.[25] This compound is an indirect band gap semiconductor with a gap of 1.7 eV, which is generally believed to be underestimated in first-principles calculations. The real gap was experimentally determined to be 2.77 eV (see the discussion part below). As expected, this compound demonstrated considerable photocatalytic activity in the following experiment.

The effects of the postannealing temperature on the structural and detailed results are determined through scanning electron microscopy (SEM) and X-ray diffraction (XRD) investigations (Figure 2). Figure 2(a)−(e) are SEM images of samples calcined at 400, 500, 600, 700, and 800 °C, respectively. Figure 2(f) shows the XRD patterns accordingly. The SEM image (Figure 2(b)) shows that particles calcined at 500 °C are plate-like with diameters of several hundred nanometers and thicknesses of 50−100 nm. Energy-dispersive spectroscopy (EDS) analysis (see inset of Figure 2(b)) confirmed that chemical composition of the particles is in a stoichiometric ratio of Bi/O/Br = 24:31:10. $Bi_{24}O_{31}Br_{10}$ grains grow up with the increase of annealing temperature. Meanwhile, agglomeration is observed when the temperature is higher than 700 °C, which is also evident by S_{BET} and pore volume results (see Supplementary Table 1 and Figure S4). With the increase of temperature, the intensity of the XRD peak increases and the full width at half-maximum of the diffraction peak narrows simultaneously, which further support particle sizes observed in SEM images. It is noteworthy that $Bi_{24}O_{31}Br_{10}$ remains in its crystal structure, and no impurity diffraction peak appears even up to 800 °C, which indicates that $Bi_{24}O_{31}Br_{10}$ is thermally stable. Referring to JCPDS card (no. 75-0888), XRD patterns demonstrate that the $Bi_{24}O_{31}Br_{10}$ sample is single phase with lattice parameters a = 10.13, b = 4.008, and c = 29.97 Å. In addition, $Bi_{24}O_{31}Br_{10}$ calcined at 500 °C shows the highest activity in degradation of rhodamine B (Rh. B) (see Supplementary Figure S2). The following experimental results shown in the main context are from the sample calcined at 500 °C. Transmission electron microscopy (TEM) and high-resolution transmission electron microscopy (HRTEM) images are shown in Figure 3. Plate-like

dx.doi.org/10.1021/cs401025u | ACS Catal. 2014, 4, 954−961

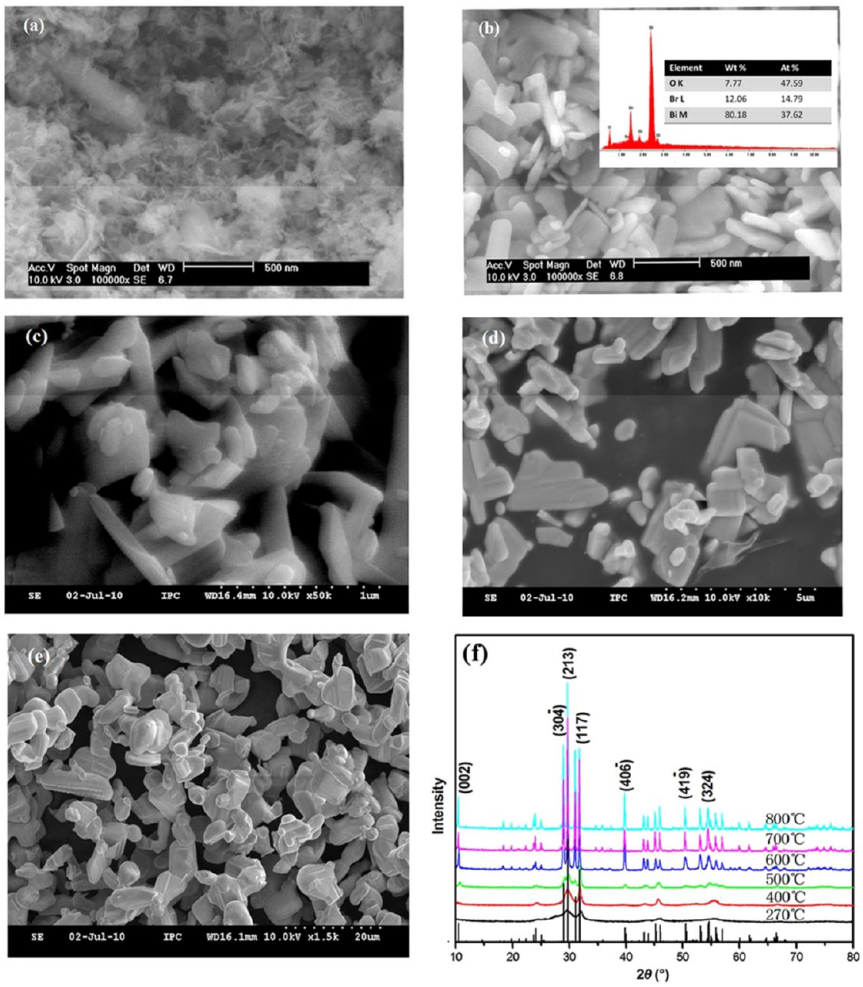

Figure 2. SEM images of $Bi_{24}O_{31}Br_{10}$ calcined at (a) 400, (b) 500, (c) 600, (d) 700, and (e) 800 °C. Inset in (b) is the EDS spectrum for $Bi_{24}O_{31}Br_{10}$ powders and (f) depicts the XRD patterns for $Bi_{24}O_{31}Br_{10}$ calcined at different temperatures, with the vertical lines marking the lines in the standard.

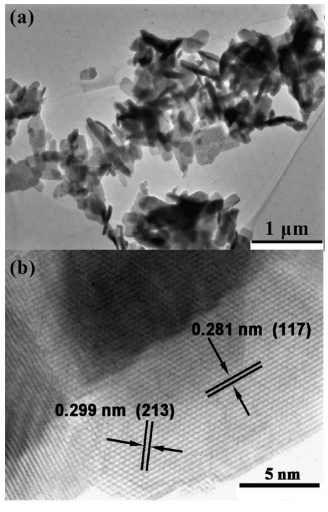

Figure 3. TEM (a) and HRTEM (b) images for $Bi_{24}O_{31}Br_{10}$ calcined at 500 °C.

morphology in TEM images agrees with the SEM results. The clear lattice fringes with an interplanar lattice spacing of 0.281 and 0.299 nm correspond to the (117), (213) atomic planes of $Bi_{24}O_{31}Br_{10}$.

The valences and orbital states of the metal ions in photocatalytic compounds have been proven to be of great importance for the photocatalytic efficiency.[30] The X-ray photoelectron spectroscopy (XPS) results demonstrate that the main peaks correspond to Bi 4f, Bi 5d, O 1s, and Br 3d orbitals for the $Bi_{24}O_{31}Br_{10}$ sample, as presented in Figure 4(a). The XPS spectrum clearly shows that Bi 5d (25.6 eV) and Br 3d (68.5 eV) states exist in core energy levels. An enlarged spectrum providing the fine details for Bi is presented in Figure 4(b), in which the peaks of Bi $4f_{7/2}$ and Bi $4f_{5/2}$ are located at 158.76 and 163.88 eV (with the splitting energy Δ = 5.12 eV), indicating that Bi ions present a valence of +3.[31]

Photocatalytic H_2 production from water under visible light is an attractive phenomenon, because H_2 can simply be formed under sunlight irradiation. Figure 5 shows the results of an H_2 production experiment using $Bi_{24}O_{31}Br_{10}$ as the photocatalyst under visible light irradiation. The constant evolution of hydrogen in water photoreduction indicates that the photocatalytic performance of $Bi_{24}O_{31}Br_{10}$ is stable during the H_2 production process driven by visible light. The total evolution of hydrogen was determined to be 133.9 μmol after 40 h, exceeding the amount of catalyst (50 mg) used in the reaction. The rate of H_2 production is 3.3 ± 0.2 μmol hour^{-1}. These results clearly show that $Bi_{24}O_{31}Br_{10}$ compound has photooxidation and photoreduction activity under the visible light

dx.doi.org/10.1021/cs401025u | ACS Catal. 2014, 4, 954−961

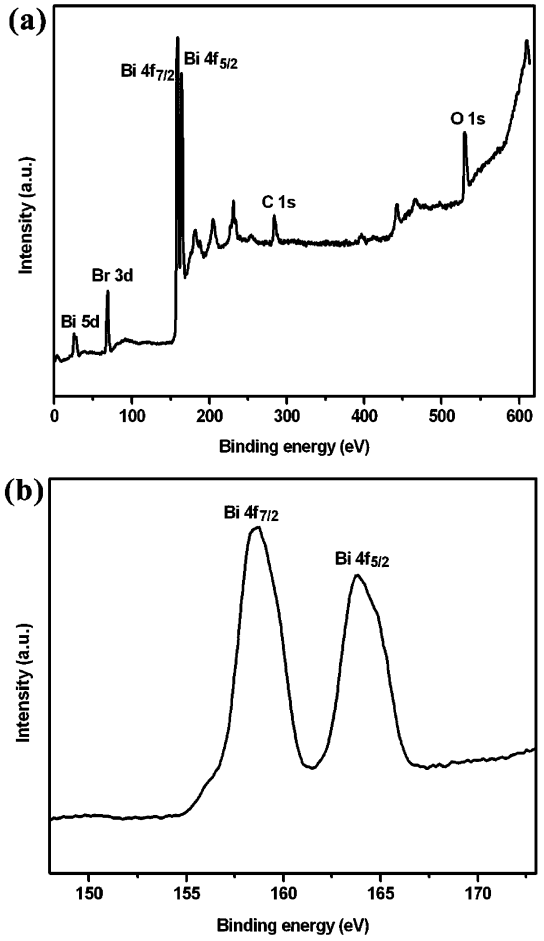

Figure 4. XPS spectra for (a) $Bi_{24}O_{31}Br_{10}$ and (b) Bi 4 f.

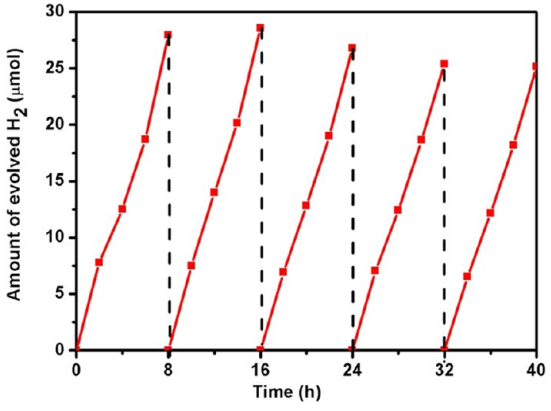

Figure 5. Cycling test of H_2 production from water under visible-light irradiation (λ > 400 nm) over $Bi_{24}O_{31}Br_{10}$ submicrometer platelets. The experiment was conducted over a 5 day period, with 40 h of overall visible light irradiation time. Methanol is the sacrificial reagent, and the anodic reaction generating O_2 from H_2O does not occur.

irradiation. The compound retains its crystal structure after photodegradation, which was confirmed by XRD analysis (shown in Supplementary Figure S3). We also tested the H_2 production using BiOBr and Bi_2O_3, and no H_2 is detected. In addition, the photoreduction of water to hydrogen under ultraviolet−visible (UV−vis) light was also carried out, and the results are shown in Supplementary Figure S5. $Bi_{24}O_{31}Br_{10}$ loaded with Ag shows the highest photocatalytic activity compared to those of pure $Bi_{24}O_{31}Br_{10}$ and P25. Here, the noble metal plays the role of cocatalyst by capturing photoinduced electrons in the surface of semiconductor and promoting the electron−hole separation, thus contributing to the high hydrogen evolution.[32] Moreover, the surface plasmon resonance (SPR) effect may further contribute to the enhancement of photocatalytic activity.[33,34]

Metal ions easily build up their concentrations in food chains to toxic levels. Carcinogenic Cr (VI) ion is a common byproduct in industries of electroplating, tanning, and dying. The effective removal of toxic Cr (VI) ions would benefit both the environment and the food chain. However, at the current time, very limited methods have been developed to eliminate such toxic ions. Here, photoreduction of Cr (VI) in water was carried out. The results are shown in Figure 6. $Bi_{24}O_{31}Br_{10}$

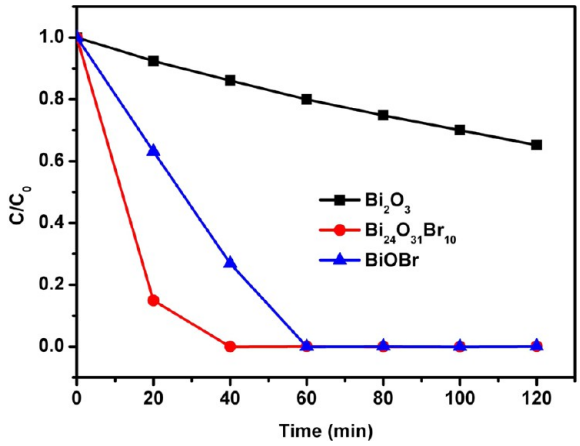

Figure 6. Comparison of photocatalytic activity for the Cr (VI) reduction experiment with Bi_2O_3, BiOBr, and $Bi_{24}O_{31}Br_{10}$.

presented the highest activity among Bi_2O_3, BiOBr, and $Bi_{24}O_{31}Br_{10}$ in the photocatalytic reduction of Cr (VI) test. The Cr (VI) ions were totally removed in 40 min for the $Bi_{24}O_{31}Br_{10}$ photocatalyst. In this experiment, $Bi_{24}O_{31}Br_{10}$ shows its potential application in environmental pollution purification. It is verified that this compound possesses not only considerable photocatalytic activity in reduction of water to H_2 but also high photocatalytic efficiency in Cr (VI) reduction.

Figure 7(a) shows a UV−vis diffuse reflectance spectrum of $Bi_{24}O_{31}Br_{10}$ powder. It reveals a clear absorption edge of 450 nm with a tail extending to 480 nm. This is consistent with the yellow color of the powder, which indicates that $Bi_{24}O_{31}Br_{10}$ could efficiently absorb visible light (Figure 7(a) inset). According to the Tauc formula,[35] an indirect band gap of 2.77 eV (Figure 7(b)) is estimated. The detailed derivation process is demonstrated in Supporting Information. The photocurrent response of $Bi_{24}O_{31}Br_{10}$ powder is shown in Figure 8(a). A reasonable current signal is detected when the visible light is on. This means that $Bi_{24}O_{31}Br_{10}$ materials can effectively generate photoinduced charge carries by absorption of visible light.[36,37] Surface photovoltage (SPV) spectroscopy is a powerful method to detect the changes of the surface potential barrier coming from effective separation of photoinduced electron−hole pairs before and after illumination.[38,39] As shown in Figure 8(b), a broad peak appears in the SPV spectrum in the UV and visible light region (300−515 nm), which indicates that the surface potential barriers of the $Bi_{24}O_{31}Br_{10}$ plates change before and after irradiation.[38−40] As a

dx.doi.org/10.1021/cs401025u | ACS Catal. 2014, 4, 954−961

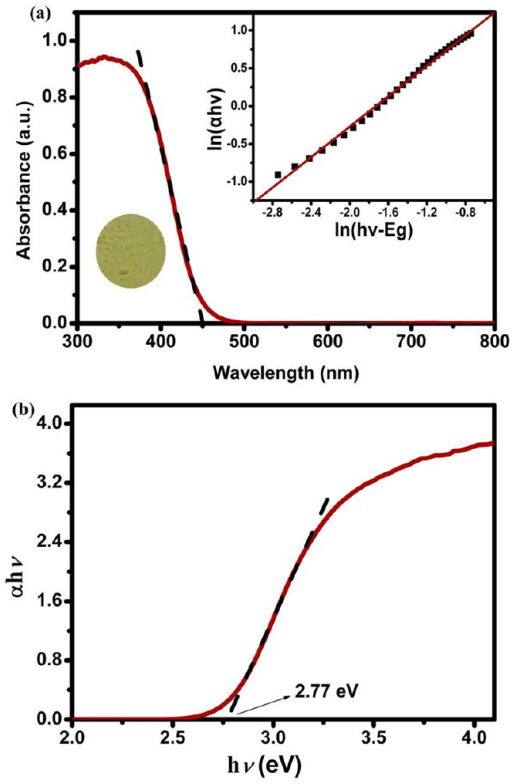

Figure 7. (a) UV−vis diffuse reflectance spectrum of $Bi_{24}O_{31}Br_{10}$ submicrometer platelets. Inset at left bottom of (a): photograph of the as-prepared photocatalyst. (b) Derivation of bandgap value (for the detailed process, see Supporting Information).

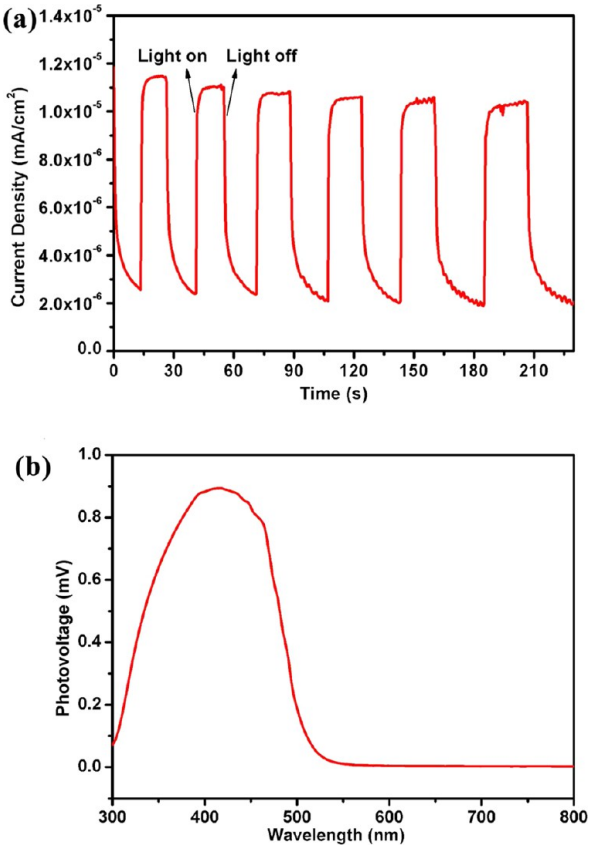

Figure 8. (a) Current density transient with light on/off for $Bi_{24}O_{31}Br_{10}$ powders under visible light (λ > 400 nm). (b) Surface photovoltage spectrum of $Bi_{24}O_{31}Br_{10}$ submicrometer platelets.

result, visible light photon absorption of $Bi_{24}O_{31}Br_{10}$ induces charge generation and separation. The maximum photovoltage is achieved at an excitation wavelength of 425 nm, which corresponds to the value of the band gap of 2.77 eV. The photocurrent response and SPV show that the $Bi_{24}O_{31}Br_{10}$ material possesses an excellent response to visible light and that the photoinduced electron−hole pairs could be separated effectively.

Based on Xu's report, the relative position of the conduction band edge can be deduced from the empirical equation:[41] $E_c = \chi - 0.5\ E_g + E_0$, where E_g is band gap, E_0 is a scale factor relating the reference electrode redox level to the absolute vacuum scale (E_0 = −4.5 eV for normal hydrogen electrode), and χ is the absolute electronegativity of semiconductor, which is the geometric mean of the electronegativity of the constituent atoms. Herein, the electronegativity of an atom is the arithmetic mean of the atomic electron affinity and the first ionization energy. Hence, the difference of the conduction band bottom between BiOBr and $Bi_{24}O_{31}Br_{10}$ could be partially attributed to the absolute electronegativity. The comparison of band edges for these two catalysts is drawn in Supplementary Figure S6. The calculated E_c of $Bi_{24}O_{31}Br_{10}$ (0.30 eV) is more negative than that of BiOBr (0.56 eV). It is important to note that this equation is empirical, theoretical, and only takes electronegativity into account. Thus, E_c calculated through this equation just has a relative value. To further elucidate the electronic structure of $Bi_{24}O_{31}Br_{10}$, electrochemical flat potential measurements were carried out, and the data were plotted in Mott−Schottky coordinates, as shown in Figure 9(a). Generally, flat-band potential values are determined using the Mott−Schottky equation.[42]

$$\frac{1}{C^2} = \frac{2}{\varepsilon\varepsilon_0 N_D}\left(E - E_{fb} - \frac{\kappa_B T}{q}\right) \quad (1)$$

where C is the space charge capacitance, N_D is the donor density, ε and ε_0 are the dielectric constants of free space and the film electrode, respectively, E is the applied potential, E_{fb} is the flat-band potential, k_B is Boltzmann's constant, T is the temperature, and q is the electronic charge. The E_{fb} value can be determined from the extrapolation to $1/C^2 = 0$. The flat potential is calculated to be −0.99 V versus the saturated calomel electrode (SCE), which is equivalent to −0.75 V versus the normal hydrogen electrode (NHE). It is known that the conduction bands of *n*-type semiconductors are 0−0.1 eV higher than the flat potentials, depending on the electron effective mass and carrier concentration.[43−45] Here, the voltage difference between the conduction band and the flat potential is set to be 0.05 eV, and the bottom of the conduction band is therefore −0.80 eV. The reduction potential of H^+/H_2 is −0.41 eV when the pH value of the electrochemical system is about 7. Figure 9(b) contains a schematic diagram of the band structure and the redox potential of $Bi_{24}O_{31}Br_{10}$ corresponding to a Mott−Schottky fitting. The negative value of the flat-band potential clearly indicates that $Bi_{24}O_{31}Br_{10}$ can effectively produce H_2 from water under irradiation.

Modulation of band structure among a series of bismuth bromine oxides is vital to improve the photocatalytic activity of bismuth oxide. Xiao's and Yu's very recent reports also support this hypothesis.[23,24] Xiao and Yu found that the degradation rates of bisphenol A (BPA) and acid orange II over $Bi_{24}O_{31}Br_{10}$

dx.doi.org/10.1021/cs401025u | ACS Catal. 2014, 4, 954−961

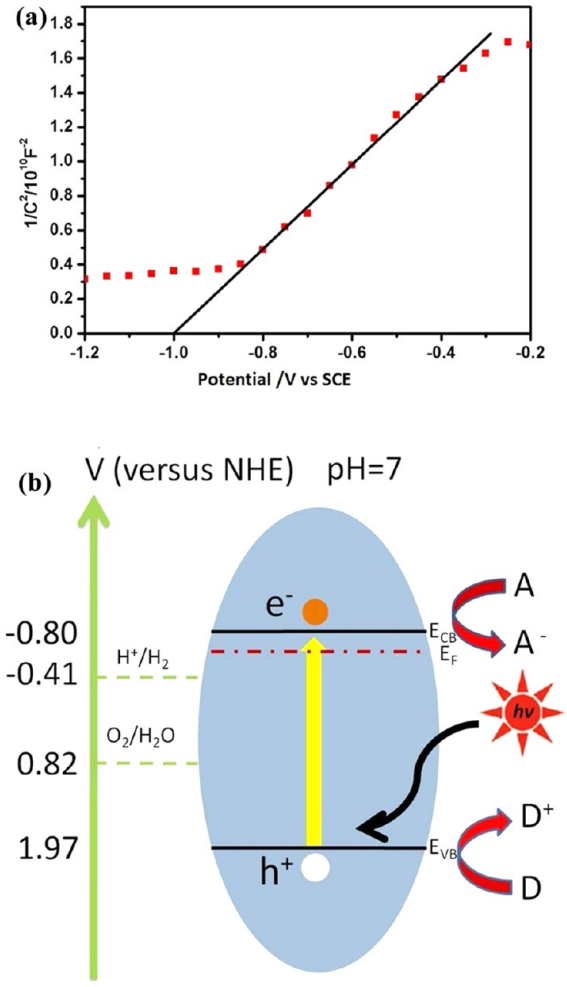

Figure 9. (a) Mott–Schottky plot for $Bi_{24}O_{31}Br_{10}$ electrode in saturated KCl solution vs SCE. (b) Schematic diagram of band gap structure and redox potential of $Bi_{24}O_{31}Br_{10}$.

catalyst under visible light irradiation are 52% in 2 h and 47% in 4 h, respectively. Their results also proved that $Bi_{24}O_{31}Br_{10}$ compound features considerable photocatalytic degradation activity. It has been proven that BiOBr shows high oxidation activity in degradation of a dye.[17,18] In photocatalytic degradation of Rh. B, the activities of $Bi_{24}O_{31}Br_{10}$, BiOBr, and Bi_2O_3 are compared and shown in Figure 10. $Bi_{24}O_{31}Br_{10}$ catalyst shows higher photo-oxidation activity than BiOBr or Bi_2O_3. However, the CB bottom of BiOBr is more positive than the electrode potential of H^+/H_2, which means that BiOBr cannot split water to release H_2.[46] In contrast to BiOBr, $Bi_{24}O_{31}Br_{10}$ shows unique reduction capability in H_2 production from water. It is considered that changes in the Bi, O, and Br proportions lead to a variation of orbital hybridization and uplifting of the bottom of the CB. With the bottom of the CB more negative than the electrode potential of H^+/H_2, water can be effectively split to H_2 under visible-light irradiation. The electronic band structure considerations also suggest a strategy in photocatalyst design. Semicondutors consisting of the p-block elements, such as In, Sn, S, O, and X (X = Cl, Br, I), due to the anisotropic properties of the p state, have light electrons or holes, which is advantageous for the photoinduced charge carrier transfer.

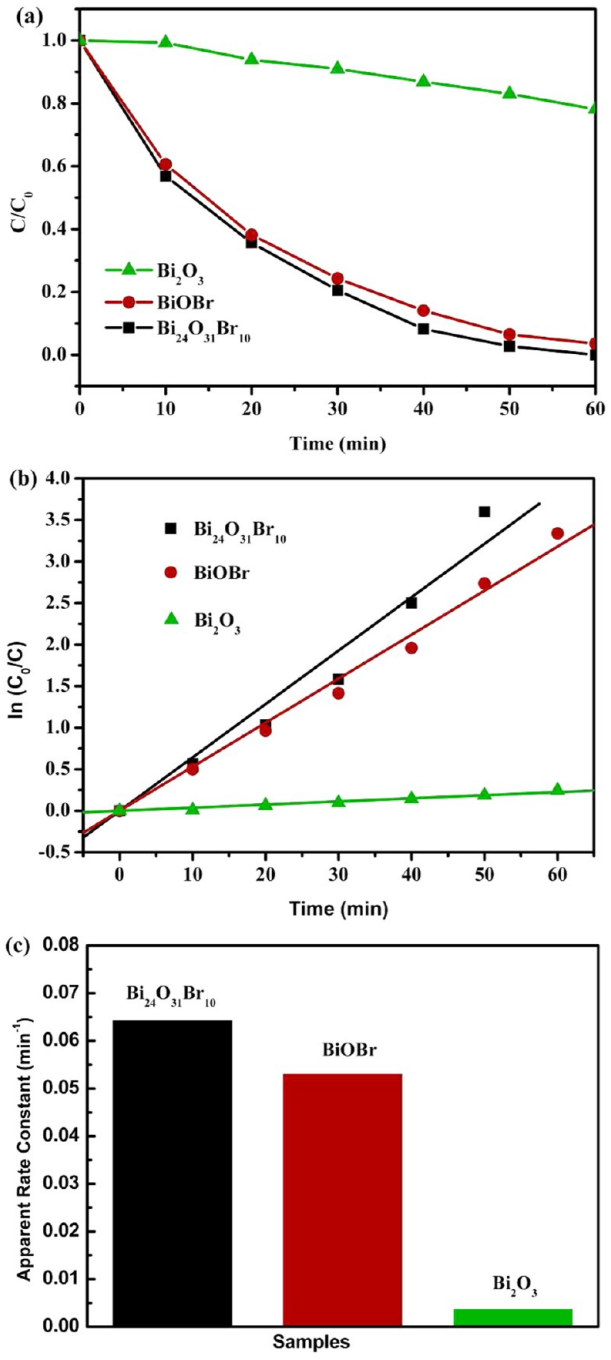

Figure 10. Decoloration of Rh. B over $Bi_{24}O_{31}Br_{10}$, BiOBr, and Bi_2O_3. (a) C/C_0–time curve. (b) $\ln(C/C_0)$–time curve. (c) Apparent rate constant of different samples.

CONCLUSIONS

In summary, we have introduced a bismuth oxybromide with considerable photocatalytic reduction activity, as proved via photoreduction of water and by a Cr (VI) ion removal test. The photoreduction capability of $Bi_{24}O_{31}Br_{10}$ in the H_2 production test is 133.9 μmol evolution of hydrogen after 40 h under visible light irradiation. During the photocatalytic reduction of Cr (VI) test, $Bi_{24}O_{31}Br_{10}$ presents the highest activity among Bi_2O_3, BiOBr, and $Bi_{24}O_{31}Br_{10}$. Compared with BiOBr, changes in the Bi, O, and Br proportions lead to variation of orbital hybridization and uplifting of the bottom of the CB. Thus, $Bi_{24}O_{31}Br_{10}$ could split water to H_2. First-principles calculations

dx.doi.org/10.1021/cs401025u | ACS Catal. 2014, 4, 954–961

indicate that the CB of $Bi_{24}O_{31}Br_{10}$ mainly consists of hybridized Bi 6p and Br 4s orbitals, which may contribute to the CB uplifting. As there are few Bi-based photocatalysts with the position of CB negative enough to split water, further research on the electronic structure of $Bi_{24}O_{31}Br_{10}$ is valuable. This research may be helpful for the exploration of new water reduction photocatalysts from the as-reported catalysts which cannot meet the electric potential requirement.

METHODS

Materials. $Bi(NO_3)_3{\cdot}5H_2O$, HNO_3, NaOH, and hexadecyl trimethyl ammonium bromide (CTAB) were purchased from Sinopharm Chemical Reagent Co., Ltd. (SCRC). The model pollutant Rh. B and $K_2Cr_2O_7$ were obtained from Beijing Chemical Reagents Company. All reagents used in this work were of analytical grade and were used as received without any further purification.

Sample Preparation. $Bi_{24}O_{31}Br_{10}$ powders were synthesized by a chemical precipitation method.[47] Initially, 2.42 g of $Bi(NO_3)_3{\cdot}5H_2O$ was dissolved in 50 mL of 1.6 M dilute nitric acid, and 0.76 g of CTAB was dissolved in 200 mL of 0.14 M NaOH aqueous solution. The alkali solution was slowly dropped into the acid solution with vigorous magnetic stirring, and a white precipitate formed at the same time. After the precipitate was purified by filtration, washed with distilled water several times, and heated at different heat-treatment temperatures (300, 400, 500, 600, 700, and 800 °C), yellow-green $Bi_{24}O_{31}Br_{10}$ powders were obtained. Ag (1 wt %) was loaded on the $Bi_{24}O_{31}Br_{10}$ surface via a photoreduction process under irradiation from a 375 W mercury lamp. A $TiO_{2-x}N_x$ reference sample was prepared by annealing TiO_2 (Degussa P25) under NH_3 atmosphere at 500 °C for 8 h.

Structure Characterization. Powder XRD patterns were collected with a PANalytical X′ Pert Pro X-ray diffractometer using Cu Kα radiation (1.54 Å), and the working voltage was 40 kV. TEM and HRTEM images were performed with a JEM-2100 high-resolution transmission electron microscope, using an accelerating voltage of 200 kV. UV−vis diffuse reflectance spectra were collected on a Cintra-10e spectrometer using $BaSO_4$ as the reference sample. The morphologies of the as-prepared samples were observed using a Hitachi SEM-CS 3400 operated at 10 kV. XPS was conducted at the Photoelectron Spectroscopy Station (Beamline 4W9B) of the Beijing Synchrotron Radiation Facility of the Institute of High Energy Physics, Chinese Academy of Sciences. Specific surface areas of samples were measured by the BET (Brunauer−Emmett−Teller) method. Nitrogen adsorption−desorption isotherms were obtained on an Autosorb iQ system (Quantachrome Instruments, USA) at liquid nitrogen temperature of 77 K. The Barrett−Joyner−Halenda (BJH) approach was used to yield mean pore size and pore size distribution from desorption data.

In the photocurrent−time response system, a 300W Xe lamp with a monochromator and a cutoff filter (λ > 400 nm) was used as the light source, and the photocurrent as a function of irradiation time under visible light was collected by a KEITHLEY 2400 source meter. The surface photovoltage (SPV) spectroscopy apparatus is composed of a source of monochromatic light, a lock-in amplifier (SR830-DSP) with a light chopper (SR540), and a photovoltaic cell. A 500 W xenon lamp (CHFXQ500W, Global Xenon Lamp Power) and a grating monochromator (Omni-5007, no. 09010, Zolix) provide monochromatic light. The construction of the photocurrent−time response cell and the photovoltaic cell was in the form of a sandwich-like structure of indium tin oxide (ITO)−sample−ITO.

The Mott−Schottky curves were collected with a PARSTAT-2273 Advanced Electrochemical System (Princeton Applied Research). The $Bi_{24}O_{31}Br_{10}$ film, Pt foil, SCE, and saturated KCl solution were used as working, counter, reference electrodes, and electrolyte, respectively. The working electrode was prepared via the dip-coating method. The Mott−Schottky measurements were monitored at a fixed frequency of 100 Hz with 10 mV amplitude at various potentials.

Photocatalytic Reactions. $K_2Cr_2O_7$ was used as the Cr (VI) source to perform the reduction of Cr (VI) test. $Bi_{24}O_{31}Br_{10}$ (50 mg) was added to the 50 mg/L $K_2Cr_2O_7$ solution. The pH value of the reaction system was adjusted to 2 using dilute sulfuric acid. The suspension was stirred under the irradiation of a 375 W mercury lamp with a filter glass (λ > 400 nm) to remove UV. The absorption spectra of $K_2Cr_2O_7$ were collected on a HITACHI U3010 UV−vis spectrophotometer.

For the photoreduction of water to hydrogen, $Bi_{24}O_{31}Br_{10}$ powder (50 mg), 20 mL of H_2O and 10 mL of methanol were placed into a 50 mL quartz tube. The cuvette was sealed with a rubber septum and degassed by bubbling N_2 for 30 min under atmospheric pressure. Then, a photocatalytic reaction took place under irradiation of a 300 W Xe lamp with a cutoff filter glass (λ > 400 nm) to remove UV. All the experiments were carried out at room temperature. The hydrogen generated from the system was measured with a GC−14C instrument (Shimadzu Co.), which was equipped with a 5 Å molecular sieve column (3 m × 2 mm), a thermal conductivity detector, and N_2 carrier gas. The amount of hydrogen was quantified by the external standard method.

In order to achieve the photo-oxidation of rhodamine B (Rh. B), the catalyst (50 mg) was added into an aqueous solution of Rh. B (0.02 mmol/L, 100 mL) in a 150 mL quartz reactor. The photocatalytic experiments were carried out under irradiation of a 300 W mercury lamp with a filter glass (λ > 420 nm) to remove UV. Prior to irradiation, the suspensions were stirred in the dark for 2 h to reach adsorption−desorption equilibrium. The absorption spectra of Rh. B were collected on a HITACHI U3010 UV−vis spectrophotometer.

First-Principles Calculations. The first-principles calculations were performed based on the plane-wave pseudopotential approach. Ultrasoft pseudopotentials and a plane wave cutoff energy of 380 eV were employed.

ASSOCIATED CONTENT

Supporting Information

Relationship between band state shape and charge carrier mobility; decoloration of Rh. B over $Bi_{24}O_{31}Br_{10}$ samples calcined at different temperatures; XRD patterns for $Bi_{24}O_{31}Br_{10}$ before and after the H_2 evolution; BET-specific surface areas, nitrogen adsorption−desorption isotherm, and pore distributions of $Bi_{24}O_{31}Br_{10}$ samples; H_2 production from water under UV−vis light irradiation over $Bi_{24}O_{31}Br_{10}$ submicrometer platelets, $Bi_{24}O_{31}Br_{10}$ sample loaded with Ag and P25; derivation process of the bandgap value from UV−vis diffuse reflectance spectrum; estimated band edges of $Bi_{24}O_{31}Br_{10}$ and BiOBr through empirical equation. This material is available free of charge via the Internet at http://pubs.acs.org.

AUTHOR INFORMATION

Corresponding Author

*E-mail: whao@buaa.edu.cn.

Author Contributions

J.S., W.C.H., and X.J.L. contributed equally to this work. W.C.H. and T.M.W. designed the experiments. J.S., X.J.L., and W.C.H. performed the experimental work and collected and analyzed the data. W.C.H., X.L.W., Y. D., and S. X. D. carried out the first-principles calculations and theoretical analysis. T.F.X. and D.J.W. were responsible for the surface potential spectrum analysis. J.O.W. carried out the XPS characterization and helped with data analysis. W.C.H., J. S., X.J.Lv, and X.L.W analyzed the data and wrote the paper.

Notes

The authors declare no competing financial interest.

ACKNOWLEDGMENTS

This work was financially supported by the National Natural Science Foundation of China (NSFC) (grant nos. 51072012,

21107117, and 51272015). X.J.Lv thanks the Beijing Natural Science Foundation (2132057). X.L.W., Y.D, and S.X.D thank the Australian Research Council (ARC) for partial support of this work through a Discovery Project (grant no. DP1094073 and DP140102581). T.M.W. and W.C.H. thank Prof. Jinhua Ye from the National Institute for Materials Science (NIMS), Japan, for valuable discussions, suggestions, and critical reading of this paper. The authors thank Dr. T. Silver for her useful discussions. W.C.H. also acknowledges financial support as a visiting scholar at the University of Wollongong from the China Scholarship Council.

REFERENCES

(1) Carey, J. H.; Lawrence, J.; Tosine, H. M. *Bull. Environ. Contam. Toxicol.* **1976**, *16*, 697−701.
(2) Mills, A.; Davies, R. H.; Worsley, D. *Chem. Soc. Rev.* **1993**, *22*, 417−425.
(3) Legrini, O.; Braun, A. M.; Oliveros, E. *Chem. Rev.* **1993**, *93*, 671−698.
(4) Hoffmann, M. R.; Martin, S. T.; Choi, W.; Bahnemann, D. W. *Chem. Rev.* **1995**, *95*, 69−96.
(5) Heller, A. *Acc. Chem. Res.* **1995**, *28*, 503−508.
(6) Zou, Z. G.; Ye, J. H.; Sayama, K.; Arakawa, H. *Nature* **2001**, *414*, 625−627.
(7) Kudo, A.; Miseki, Y. *Chem. Soc. Rev.* **2009**, *38*, 253−278.
(8) Osterloh, F. E. *Chem. Mater.* **2008**, *20*, 35−54.
(9) Ione, T.; Fujishima, A.; Konishi, S.; Honda, K. *Nature* **1979**, *277*, 637−638.
(10) Liu, Q.; Zhou, Y.; Kou, J.; Chen, X.; Tian, Z.; Gao, J.; Yan, S.; Zou, Z. *J. Am. Chem. Soc.* **2010**, *132*, 14385−14387.
(11) Kudo, A.; Omori, K.; Kato, H. *J. Am. Chem. Soc.* **1999**, *121*, 11459−11467.
(12) Oshikiri, M.; Boero, M.; Ye, J.; Zou, Z.; Kido, G. *J. Chem. Phys.* **2002**, *117*, 7313−7318.
(13) Sillén, L. G. *Z. Anorg. Allg. Chem.* **1941**, *246*, 115−130.
(14) Ueda, W.; Isozaki, T.; Sakyu, F.; Nishiyama, S.; Morikawa, Y. *Bull. Chem. Soc. Jpn.* **1996**, *69*, 485−491.
(15) Kusainova, A. M.; Lightfoot, P.; Zhou, W. *Chem. Mater.* **2001**, *13*, 4731−4737.
(16) Maile, F. J.; Pfaff, G.; Reynders, P. *Prog. Org. Coat.* **2005**, *54*, 150−163.
(17) Zhang, X.; Ai, Z.; Jia, F.; Zhang, L. *J. Phys. Chem. C* **2008**, *112*, 747−753.
(18) An, H. Z.; Du, Y.; Wang, T. M.; Wang, C.; Hao, W. C.; Zhang, J. Y. *Rare Met.* **2008**, *27*, 243−250.
(19) Gnayem, H.; Sasson, Y. *ACS Catal.* **2013**, *3*, 186−191.
(20) Kako, T.; Zou, Z.; Katagiri, M.; Ye, J. *Chem. Mater.* **2007**, *19*, 198−202.
(21) Yao, W. F.; Xu, X. H.; Wang, H.; Zhou, J. T.; Yang, X. N.; Zhang, Y.; Shang, S. X.; Huang, B. B. *Appl. Catal., B* **2004**, *52*, 109−116.
(22) Yao, W. F.; Wang, H.; Xu, X. H.; Cheng, X. F.; Huang, J.; Shang, S. X.; Yang, X. N.; Wang, M. *Appl. Catal., A* **2003**, *243*, 185−190.
(23) Xiao, X.; Liu, C.; Hu, R.; Zuo, X.; Nan, J.; Li, L.; Wang, L. *J. Mater. Chem.* **2012**, *22*, 22840−22843.
(24) Yu, C. L.; Zhou, W. Q.; Yu, J.; Cao, F. F.; Li, X. *Chin. J. Chem.* **2012**, *30*, 721−726.
(25) Umezawa, N.; Ouyang, S. X.; Ye, J. H. *Phys. Rev. B* **2011**, *83*, 035202.
(26) Wang, X. L. *Phys. Rev. Lett.* **2008**, *100*, 156404.
(27) Vurgaftman, I.; Meyer, J. R.; Ram-Mohan, L. R. *J. Appl. Phys.* **2001**, *89*, 5815 −5875.
(28) Santander-Syro, A. F.; Copie, O.; Kondo, T.; Fortuna, F.; Pailhès, S.; Weht, R.; Qiu, X. G.; Bertran, F.; Nicolaou, A.; Taleb-Ibrahimi, A.; Fèvre, P. L.; Herranz, G.; Bibes, M.; Reyren, N.; Apertet, Y.; Lecoeur, P.; Barthélémy, A.; Rozenberg, M. J. *Nature* **2011**, *469*, 189−193.
(29) Eggenweiler, U.; Keller, E.; Kraemer, V. *Acta Crystallogr., Sect. B: Struct. Sci.* **2000**, *56*, 431−437.
(30) Hosogi, Y.; Shimodaira, Y.; Kato, H.; Kobayashi, H.; Kudo, A. *Chem. Mater.* **2008**, *20*, 1299−1307.
(31) Ai, Z. H.; Ho, W. K.; Lee, S. C.; Zhang, L. Z. *Environ. Sci. Technol.* **2009**, *43*, 4143−4150.
(32) Henglein, A. *J. Phys. Chem.* **1979**, *83*, 2209−2216.
(33) Awazu, K.; Fujimaki, M.; Rockstuhl, C.; Tominaga, J.; Murakami, H.; Ohki, Y.; Yoshida, N.; Watanabe, T. *J. Am. Chem. Soc.* **2008**, *130*, 1676−1680.
(34) Cushing, S. K.; Li, J.; Meng, F.; Senty, T. R.; Suri, S.; Zhi, M.; Li, M.; Bristow, A. D.; Wu, N. *J. Am. Chem. Soc.* **2012**, *134*, 15033−15041.
(35) Butler, M. A. *J. Appl. Phys.* **1977**, *48*, 1914−1920.
(36) Lv, X. J.; Zhou, S. X.; Zhang, C.; Chang, H. X.; Chen, Y.; Fu, W. F. *J. Mater. Chem.* **2012**, *22*, 18542−18549.
(37) Lv, X. J.; Fu, W. F.; Chang, H. X.; Zhang, H.; Cheng, J. S.; Zhang, G. J.; Song, Y.; Hu, C. Y.; Li, J. H. *J. Mater. Chem.* **2012**, *22*, 1539−1546.
(38) Kronik, L.; Shapira, Y. *Surf. Sci. Rep.* **1999**, *37*, 1−206.
(39) Lin, Y. H.; Wang, D. J.; Zhao, Q. D.; Yang, M.; Zhang, Q. L. *J. Phys. Chem. B* **2004**, *108*, 3202−3206.
(40) Xie, T. F.; Wang, D. J.; Zhu, L. J.; Li, T. J.; Xu, Y. J. *Mater. Chem. Phys.* **2001**, *70*, 103−106.
(41) Xu, Y.; Schoonen, M. A.A. *Am. Mineral.* **2000**, *85*, 543−556.
(42) Bott, A. W. *Curr. Sep.* **1998**, *17*, 87−91.
(43) Luo, W. J.; Li, Z. S.; Jiang, X. J.; Yu, T.; Liu, L. F.; Chen, X. Y.; Ye, J. H.; Zou, Z. G. *Phys. Chem. Chem. Phys.* **2008**, *10*, 6717−6723.
(44) Wang, J. L.; Yu, Y.; Zhang, L. Z. *Appl. Catal., B* **2013**, *136−137*, 112−121.
(45) Xiao, X. Y.; Jiang, J.; Zhang, L. Z. *Appl. Catal., B* **2013**, *142−143*, 487−493.
(46) Wang, W. D.; Huang, F. Q.; Lin, X. P.; Yang, J. H. *Catal. Commun.* **2008**, *9*, 8−12.
(47) Deng, H.; Wang, J. W.; Peng, Q.; Wang, X.; Li, Y. D. *Chem.—Eur. J.* **2005**, *11*, 6519−6524.